IOSR Journal of Electronics and Communication Engineering (IOSR-JECE)
e-ISSN: 2278-2834, p- ISSN: 2278-8735.Volume 20, Issue 6, Ser. I (Nov – Dec 2025), PP 81-89
www.iosrjournals.org

Design And Thermal Modelling Of Induction Motor For Prolong Lifespan

Asuquo Eke, O. I. Okoro, A. J. Onah, E. J. Akpama
Department Of Electrical/Electronic Engineering, Cross River University Of Technology, Calabar. Nigeria
Department Of Electrical/Electronic Engineering, Michael Okpara University Of Agriculture, Umudike. Abia State. Nigeria
Department Of Electrical/Electronic Engineering, Michael Okpara University Of Agriculture, Umudike. Abia State. Nigeria
Department Of Electrical/Electronic Engineering, Cross River University Of Technology, Calabar. Nigeria

Abstract
In order to increase the lifespan of induction motors by better electromagnetic design and improved thermal management, this study offers a thorough design and thermal modeling technique. The study precisely forecasts temperature distribution and locates possible hotspots inside the motor by combining lumped parameter thermal networks (LPTN) with finite element analysis (FEA). Air-gap optimization, slot and winding layout, and suitable material selection are important design factors that enhance heat dissipation and lower thermal stress. Effective cooling considerably reduces winding temperature rise, improves insulation durability, and extends total motor lifespan, according to electro-thermal models used to assess temperature behavior under various load circumstances. The maximum winding temperature, according to the thermal modeling results, was about 93.4 °C, securely below the Class B insulation limit of 130 °C. Despite localized hotspots around the stator and rotor cores, air cooling provides effective thermal stability, confirming the cooling system's sufficiency. Strong heat transmission through the motor yoke surfaces and few thermal limitations were demonstrated by the heat-flow study, which reached steady-state convergence at about 1.5 seconds. Strong torque characteristics with high transient peaks and little variability were found by dynamic performance study. Operational efficiency ranged from 80% to 85%, according to additional efficiency research. Overall, the study shows that the development of robust, dependable, and energy-efficient induction motors appropriate for industrial and traction applications is supported by the combination of optimum design parameters with precise multi-domain thermal modeling.

Keyword: *Induction Motor, Thermal Modelling, Motor Design, Heat Dissipation, Lifespan*

Date of Submission: 05-12-2025 Date of Acceptance: 15-12-2025

I. Introduction

Because of their sturdy design, affordability, high dependability, and ease of maintenance, induction motors are the most used electric devices in both commercial and industrial settings. Because of their adaptability, they are essential for powering mechanical loads like fans, compressors, pumps, and conveyors. However, one of the main issues with induction motors' long-term operation is their thermal performance, which has a big impact on lifespan, durability, and efficiency. One of the most important causes of insulation deterioration, winding failures, and bearing damage in induction motors is thermal stress. An excessive increase in temperature inside the motor, frequently brought on by overloads, poor ventilation, or harmonics, can hasten the deterioration of insulation materials, lower operational effectiveness, and cause early motor failure. Therefore, in order to improve the design of induction motors and increase their operating lifespan, it is crucial to comprehend and precisely simulate their thermal behavior. Electrical and mechanical considerations have historically dominated motor design, with thermal considerations frequently addressed as post-design validation. However, thermal modeling now needs to be incorporated into the design stage due to the growing demand for dependable and energy-efficient motors. Under diverse loading and environmental conditions, this method enables engineers to forecast the temperature distribution within a variety of components, including the rotor, core, stator windings, and bearings [1, 2, 3Lumped Parameter Thermal Network (LPTN) models, Computational Fluid Dynamics (CFD), and Finite Element Analysis (FEA) are examples of contemporary thermal modeling methodologies. These techniques aid in the simulation and analysis of the motor's internal heat generation and dissipation processes, taking radiation, convection, and conduction into account. Incorporating thermal restrictions into the design process allows for better material selection, cooling system optimization, and safe operating temperature maintenance. This study intends to evaluate the impact of integrated thermal design on the longevity of induction motors. Through modeling and simulation, the research analyzes how improved thermal management might decrease hotspots,

boost insulation life, and assure continuous and safe motor operation over extended periods. The case study offers useful insights for motor makers, maintenance engineers, and system designers by concentrating on induction motors that are frequently utilized in industrial settings [4]. Due to the increased demands for energy economy and dependability in contemporary electrical systems, induction motor performance and longevity have been the subject of intensive research for decades, with a growing emphasis on thermal modeling. Many research has looked into the effects of thermal stress on motor degradation, including the degradation of bearing lubrication, rotor bars, and winding insulation all of which are directly impacted by an increase in motor temperature. [5] found that about 55% of all induction motor failures are due to insulation deterioration brought on by thermal aging. The requirement for precise temperature prediction and control is further supported by IEEE and NEMA standards, which show that insulation life is lowered by around 50% for every 10°C increase above the authorized working temperature. Instead of treating thermal concerns as a secondary concern, this has led researchers to incorporate thermal limitations into the motor design phase. The thermal behavior of induction motors has been modeled using a variety of techniques. Because of its ease of use and quick computation, the Lumped Parameter Thermal Network (LPTN) model is popular and appropriate for real-time applications. Finite Element Analysis (FEA), on the other hand, provides greater precision by capturing intricate temperature gradients, particularly in intricate motor designs. After comparing the two approaches, research by [6] came to the conclusion that hybrid approaches can increase reliability by utilizing the advantages of both. Recent research has increasingly focused on integrating mechanical, thermal, and electromagnetic modeling. In [7], a co-simulation platform was proposed to link dynamic thermal behavior with electromagnetic torque analysis, enabling engineers to monitor how varying loads influence motor temperature in real time. Such coupled simulations are essential for optimizing designs under variable load conditions. Effective heat management also depends heavily on material selection. Advanced materials such as copper conductors, epoxy-mica insulation, and laminated silicon steel enhance both thermal conductivity and resistance. Furthermore, studies have highlighted the benefits of heat pipe-based cooling systems, liquid cooling, and forced-air cooling in improving heat dissipation, especially in high-power motors. Research in [4, 7] demonstrated that optimizing fin geometry on motor casings can reduce core temperatures by up to 20%. In industrial applications, predictive maintenance now leverages infrared (IR) thermography, digital twin technology, and thermal sensors. These tools enable operators to continuously monitor motor conditions, detect abnormal temperature patterns, and anticipate potential failures. Integrating these methods with accurate thermal models supports smarter decision-making regarding motor operation, maintenance, and replacement schedules. Estimating the service life of an induction motor remains vital for ensuring reliability, safety, cost efficiency, and effective maintenance planning, as it depends on a complex interplay of electrical, thermal, mechanical, and environmental factors [1, 5, 10].

II. Design Of Induction Motor For Prolong Lifespan

Designing an induction motor for extended lifespan requires minimizing thermal and mechanical stresses as well as electrical losses. Achieving this goal involves optimizing critical parameters based on fundamental design equations that define electromagnetic behavior, heat generation, and cooling performance [11, 12, 13].

Power equation

$$P_{out} = \sqrt{3} \cdot V \cdot I \cdot \cos\phi \cdot \quad (1)$$

Synchronous speed

$$N_s = \frac{120 \cdot f}{P} \quad (2)$$

Where f is supplying frequency (Hz), P is number of poles

The slip equation is

$$s = \frac{N_s - N_r}{N_s} \quad (3)$$

Magnetic Loading

Average air-gap flux density

$$B_{av} = \frac{\phi}{\pi D_s L} \quad (4)$$

Where ϕ\ph is air-gap flux per pole, Typical range: 0.45 – 0.65 T

Electrical loading

$$A = \frac{I_z \cdot Z}{\pi D_s} \quad (5)$$

Where $C_0 = \frac{\pi^2}{2} \cdot B_{av} \cdot A \cdot k_w \cdot \eta \cdot 10^{-3}$, Ds is stator bore diameter, L is core length, n is speed in rps

A correction factor is used to determine the air-gap permeance in electrical devices, mainly induction motors having air gaps. It accounts for the slotting effect in the stator and rotor's iron cores, which causes the slots

to produce an unequal air-gap flux density. The air gap between the stator and rotor is constant, and the magnetic flux is distributed equally. On the other hand, real machines have slotted rotor and stator cores to accommodate windings. These slots effectively increase the magnetic resistance of the air gap by disrupting the uniform flux distribution. By replacing the actual air gap with an equivalent uniform air gap that has the same magnetic effect, engineers may account for this impact using Carter's coefficient. Carter's coefficient kc can be computed as follows for a single slotted surface: [14]

$$k_c = \frac{\tau_s}{\tau_s - \gamma g} \quad (6)$$

If both the rotor and the stator are slotted, the total Carter's coefficient is as follows: γ is the slot opening factor (which depends on the slot design), g is the actual air gap length, and τs is the slot pitch (the center-to-center distance between two adjacent slots).

$$k_c = k_{cs} \cdot k_{cr} \quad (7)$$

Where kcs = Carter's coefficient for stator slots, kcr = Carter's coefficient for rotor slots

For slot Opening Factor γ is calculated using the geometry of the slots. A simplified empirical expression often used is

$$\gamma = \frac{2}{\pi} \ln\left(\frac{1}{\tan\left(\frac{\pi b}{2\tau_s}\right)}\right) \quad (8)$$

Where b = width of the slot opening, τs = slot pitch. This formula varies depending on the slot shape (rectangular, trapezoidal, etc.), so for precise design, accurate geometric modelling or FEA is recommended. [1, 2]

Airgap Flux density

$$B_g = \frac{\phi \cdot p}{\pi \cdot D_s \cdot L} \text{ or} \quad (9)$$

where N is the number of turns per phase, I is the current per phase (A), g is the air gap length (m), μ0 is the permeability of empty space (4π x 10^-7 H/m), Bg is the air gap flux density (Tesla), and kc is Carter's coefficient (which takes into consideration how slot openings affect the air gap flux). Additionally, the flux pole equation is

$$\phi = \frac{E \cdot 60}{4.44 \cdot f \cdot T \cdot m} \quad (10)$$

Where E = induced phase voltage, f = frequency, T = turns per phase, m = number of phases

Motor Torque Equation

The air gap and flux density are two elements that engineers should maximize while developing an electric machine. The air gap flux density can be raised by reducing the air gap length, however doing so raises the possibility of mechanical problems and magnetic saturation. The air gap flux density can be raised by increasing the number of turns, but the winding's resistance and reactance also rise. Achieving the intended air gap flux density while reducing losses can be facilitated by optimizing the current density. [17, 18] is the motor torque equation.

$$T = \frac{3}{\omega_s} \cdot \frac{R_r' s V_1^2}{\left[\left(R_1 + \frac{R_r'}{s}\right)^2 + \left(X_1 + X_r'\right)^2\right]} \quad (11)$$

Where R1, X1 = stator resistance and reactance, 'Rr′,Xr′ = rotor resistance and reactance (referred to stator), s = slip, ωs = synchronous angular speed, V1 = stator voltage. The power loss equation is given by

$$P_{loss} = P_{cu1} + P_{cu2} + P_{core} + P_{mech} \quad (12)$$

Where Pcu1 is 31^2 R is stator copper loss, P{cu2} = 3 I^2R2is the rotor copper loss, P_{core} is core loss (hysteresis + eddy current), P_{mech} is mechanical loss (friction, windage)

Thermal Modelling

the motor as a lumped thermal network using thermal resistances and capacitances as

$$C_{th} \cdot \frac{dT(t)}{dt} + \frac{T(t) - T_{amb}}{R_{th}} = P_{loss}(t) \quad (13)$$

Where C_{th}= thermal capacitance (J/K), R_{th} = total thermal resistance (K/W), T(t) = motor temperature, T_{amp} is ambient temperature, Ploss(t) = instantaneous total power losses. Solving this differential equation gives you the temperature profile over time.

Steady-State Temperature [15, 16, 17]

$$T_{steady} = T_{amb} + P_{loss} \cdot R_{th} \quad (14)$$

Lifespan Estimation

Insulation degradation doubles for every 10°C increase above the rated temperature (IEEE/IEC standard). According to Arrhenius equation

$$L = L_0 \cdot 2^{-\frac{T-T_{ref}}{10}} \quad (15)$$

Where L_0 = rated lifespan at Tref (e.g., 100,000 hours at 100°C), T = actual operating temperature

III. Results And Discussion

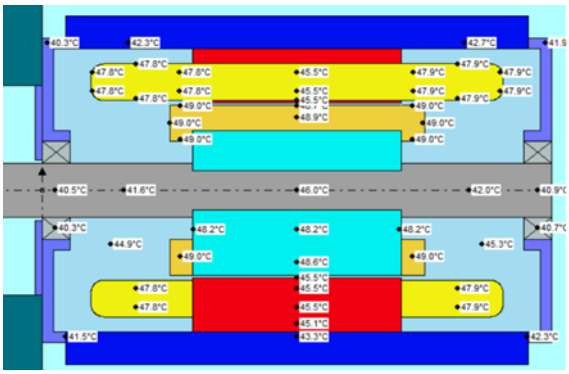

Figure. 1 graph of temperature distribution

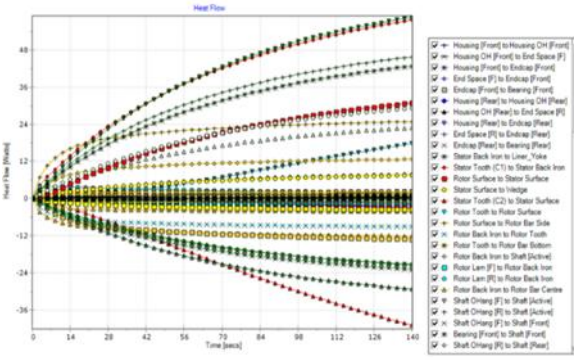

Figure. 2 graph of heatflow against time in axial view

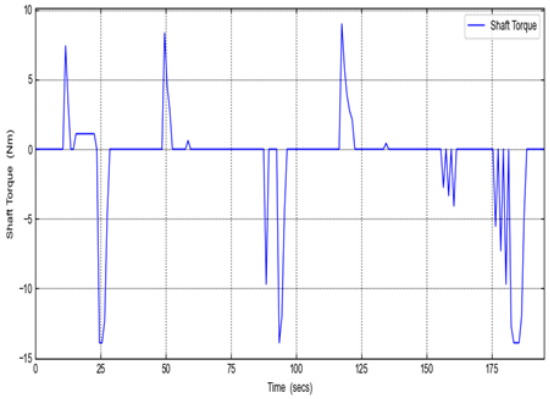

Figure. 3 graph of sharft torque against time

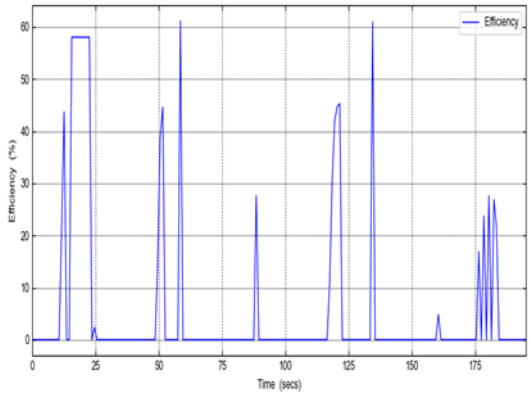

Figure. 4 graph of efficiency

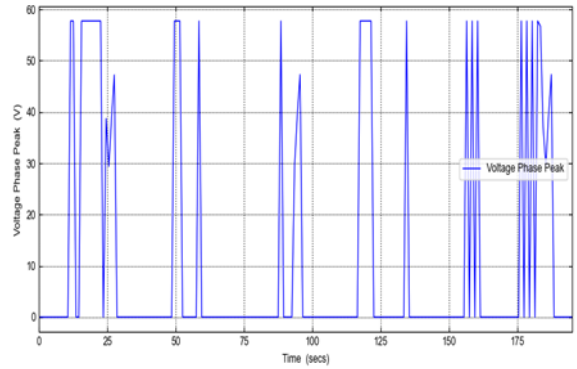

Figure. 5 graph of voltage phasepeak against time

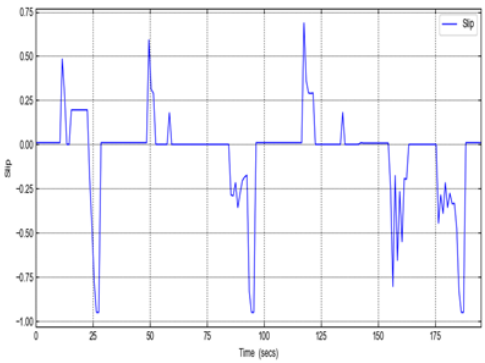

Figure. 6 graph of slip against time against time

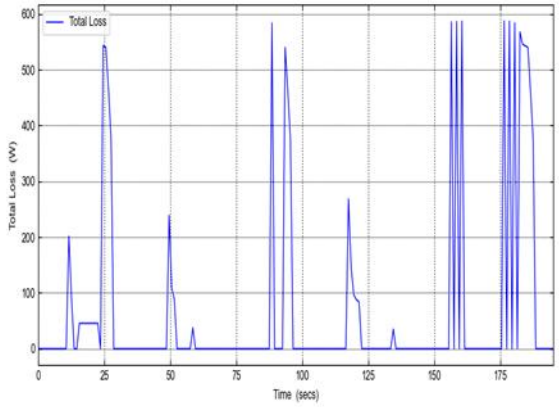

Figure.: 7 graph of total loss against time

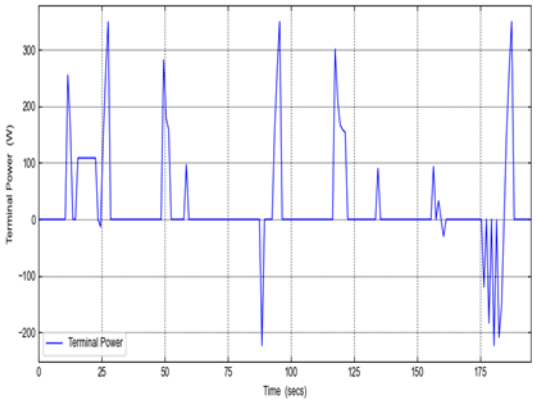

Figure.: 8 graph of terminal power against time

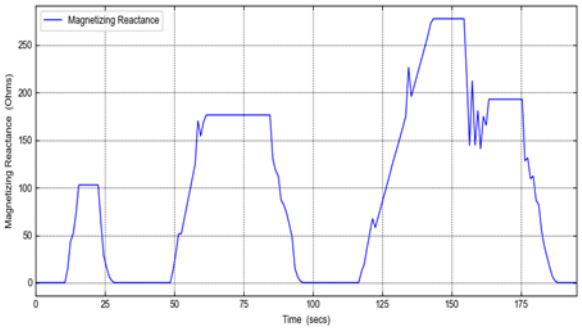

Figure.: 9 graph of magnetizing reactanace against time

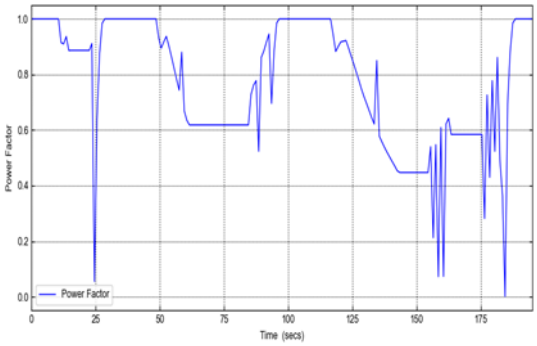

Figure.: 10 graph of power factor against time

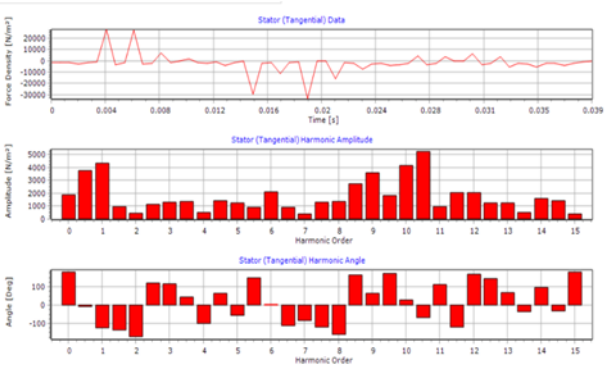

Figure.: 11 graph of force density, applitude and angle against amplitde, harmonic angle and order(stator tangential view) order(stator tangential view)

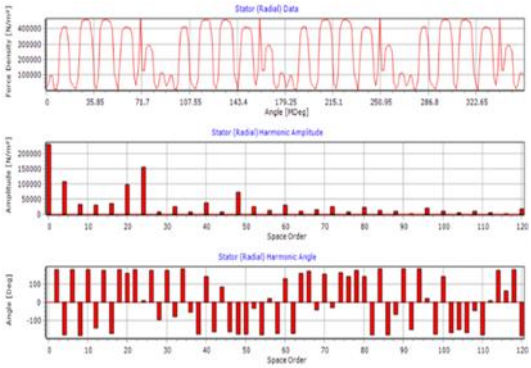

Figure.: 12 graph of force density, applitude and angle against amplitde, harmonic angle and space order (stator tangentialview)

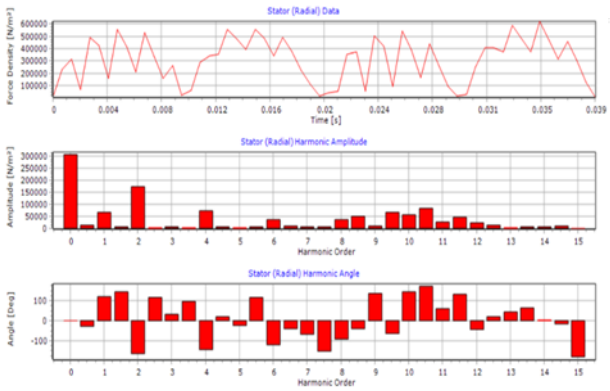

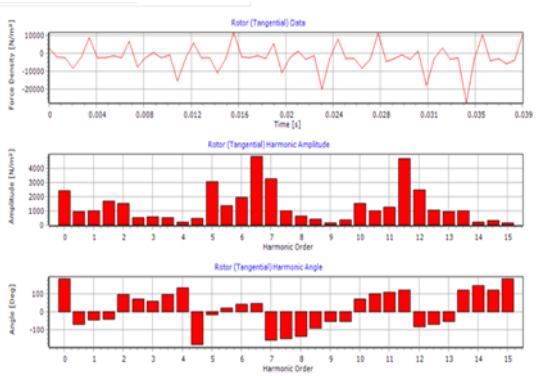

Figure.: 13 graph of force density, applitude and angle against amplitde, harmonic angle and order(stator tangential view)

Figure.: 14 graph of force density, applitude and angle against amplitde, harmonic angle and space **order(stator tangential view)**

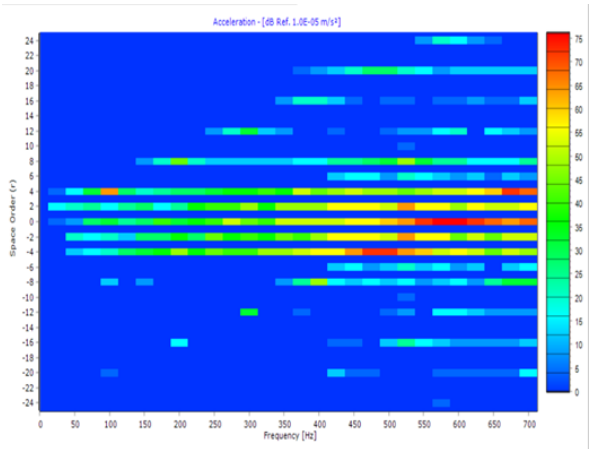

Figure.: 15 graph of space order

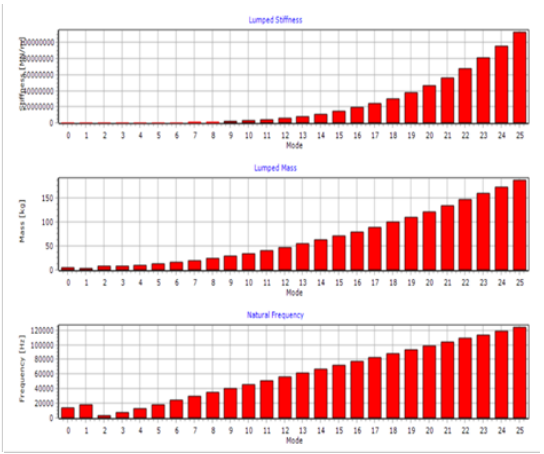

Figure.: 16 graph of lumped stiffness against frquency

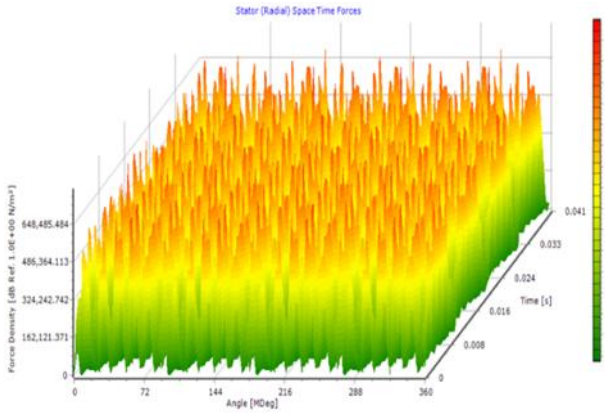

Figure.: 17 graph of force density against angle in 3D View

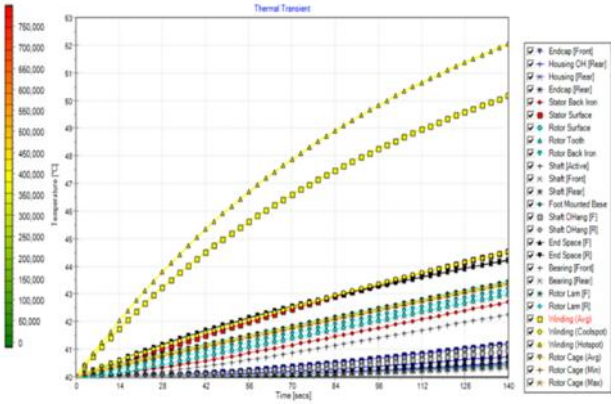

Figure.: 18 graph of temperature distribution

IV. Results Discussion

Figure 1 show the axial view temperature distribution graph, a thermal map of the induction motor's axial segment is displayed in this figure 1. The colored areas depict the temperature distribution, colder portions are depicted in blue, and hotter places in the stator core and windings are indicated in red or orange. This aids in locating heat hotspots where copper losses and insulation stress are concentrated. The significance of cooling design and the way heat moves through the motor structure are emphasized. Figure 2 is graph of heat flow against time. The heat flow changes over time across various motor parts is depicted in this image. Different motor parts are represented by multiple lines (for instance stator winding, rotor, core, housing). As the machine operates longer, the graphs demonstrate a steady increase in heat flow that eventually stabilizes at steady state. This demonstrates how losses are transferred as heat into the materials around them, which is directly related to the temperature increase depicted in Figure 1. The shaft torque versus time graph is shown in Figure 3. The instantaneous shaft torque variation is displayed in this graph. Significant swings in torque, both positive and negative, suggest oscillations, supply disruptions, or temporary loading situations. Under a constant load, torque should ideally be very smooth; variations in this regard point to instability or dynamic events (faults, abrupt load changes, or startup). The motor's efficiency curve is displayed over time in Figure 4 is a graph of Efficiency against time. Sharp peaks and valleys in efficiency are strongly associated with changes in torque, power, and losses. Efficiency sharply declines during unstable operation, demonstrating the significant impact of losses, slip changes, and voltage disturbances. This emphasizes how difficult it is to maintain high efficiency in less-than-ideal supply circumstances. The voltage phase peak is plotted versus time in Figure 5, which displays the voltage phase peak value with time. With sporadic drops and rises, the waveform exhibits significant fluctuation, which

may indicate switching events or voltage instability. The abrupt changes suggest that the motor is experiencing intermittent disruptions or fluctuating input supplies. Figure 6, Slip vs Time Graph In an induction motor, slip quantifies the variation between synchronous and rotor speeds. The plot shows that the motor is experiencing dynamic operating conditions (load fluctuations, instability, or fault-like disturbances) because of the frequent variations in slip, which can be either positive or negative. Under normal load conditions, a steady motor should have slip between 0 and 0.05; significant deviations indicate transient operation. Figure7, Total Loss Graph vs Time This is the sum of the motor's losses (windage, friction, stray loss, core loss, and copper loss). The plot displays sporadic spikes that correspond to the voltage and slip problems seen. Unstable voltage causes a sharp rise in losses. Figure.8, Terminal Power versus Time Graph. The motor's output power at the terminals is displayed in this plot. Power fluctuations point to unstable operating conditions that may be caused by changes in load or disruptions in the supply. Voltage dips or motor stalling could be the cause of the abrupt dips. Figure 9 is Magnetizing Reactance Graph with Time. The motor's capacity to create flux is shown by the magnetizing reactance, which is connected to the magnetizing branch of the equivalent circuit. The oscillations point to changes in magnetic conditions brought on by load disruptions or unstable voltage. The reactance of a stable motor would be relatively consistent. Figure 10 is Power Factor versus Time Graph. The ratio of apparent power to real power is known as the power factor. The oscillations demonstrate that the motor alternates between operating inefficiently (lower PF) and efficiently (higher PF). High-loss or transient circumstances are correlated with low power factor spots. Figure 11 Magnetizing Reactance Graph vs Time, the plot displays the magnetizing reactance mean and distribution. It draws attention to the reactance's distribution over several time periods, demonstrating its variability and potential clustering at particular ranges. Figure 12, Power Factor versus Time Graph a figure based on a histogram that displays the distribution of power factor values across time. It highlights the range of PF values, demonstrating the significant difference between bad and good PF situations. Magnetizing Reactance Graph vs Time Figure 13. It supports magnetizing reactance's dynamic and irregular nature. The power factor vs time graph in Figure 14 illustrates how the motor functions at various efficiency levels, once more indicating an inconsistent supply and load. Figure 15 Color Map/Heatmap of Magnetizing Reactance versus Time. This graphic shows the magnetizing reactance across time, frequency, and operational states in a two-dimensional color-coded heatmap. Darker regions indicate lower intensity/reactance values, while brighter colors indicate higher values. It shows clusters of stability and instability and lets you see the dynamic evolution of magnetizing reactance. Figure 16 is power factor versus Time Graph. Power factor values are displayed as a bar graph. displays a progressive distribution and a potential long-term trend. validates the previously noted variations in a more pronounced cumulative fashion. Figure 17 is 3D Surface Plot of Magnetizing Reactance versus Time A three-dimensional surface plot that illustrates the relationship between operating frequency/speed and magnetizing reactance over time. The vertical spikes imply that the magnetizing tendency fluctuates quickly. Green/blue regions indicate lower reactance levels, whilst yellow/orange peaks indicate higher values. Compared to the previous 2D reactance plots, this figure offers a more thorough picture, emphasizing both frequency-dependent and temporal fluctuations. Figure.18 is Power Factor versus Time Graph The trend of power factor fluctuation over time for various test scenarios and operating settings is displayed in this multi-curve diagram. The power factor progression under a particular load or operating situation is represented by each colored curve. Although the rate of increase varies from case to instance, the overall trend indicates that power factor increases with time and load. This demonstrates that efficiency, magnetizing reactance behavior, and operating conditions all have a significant impact on PF. The following graphs show the dynamic performance profile of an induction motor: The motor warms up as expected and distributes heat effectively. In mechanical and electrical systems, there are fluctuations and transients in torque, voltage, efficiency, and slip. Such behavior indicates the need for improved thermal management, control strategy, or system tuning, especially for applications that require steady operation, such as automation or traction. The dynamic behavior of the structure, which is most likely a part of an electric machine, is well understood thanks to these three modal plots. Stiffness and frequency increase with the number of modes. The sluggish increase in mass engagement indicates the structurally relevant modes. Reduction of vibrations, avoidance of resonance, and preservation of mechanical integrity all depend on these insights. These determine how the system responds to varying demands. The high mass and stiffness of a mode significantly affect the system's overall dynamic behavior. Extremely low frequency modes may indicate stiff body motion or global deflection. Even though high-frequency modes may not be activated during normal operation, they are essential for shock, noise, and resonance analysis. It is essential to ensure that the working frequencies of the motor or mechanical system do not coincide with natural frequencies in order to avoid resonance. These graphs can guide structural strengthening (if stiffness is low) or mass optimization (to reduce weight without compromising performance). Weak regions that are susceptible to dynamic fatigue may be indicated by modes with high mass but low rigidity. The third, fifth, and seventh harmonics which cause noise, overheating, and torque ripple are among the harmonic distortions that can be identified with the use of these graphs. Uneven or high harmonic amplitudes could be an indicator of issues with the supply's quality or the magnetic design [1, 2]. illustrates the rotor's reaction to stator field influences as well as its own generated currents. Harmonic distortions

in the rotor can be a sign of electromagnetic noise, slip fluctuation, and torque ripple. The frequency-dependent vibrations of many modes are depicted in this vibration spectrogram. helps determine resonance conditions and crucial frequencies that should be avoided in design or operation. Rigidity and mass are increased by higher modes. Higher natural frequencies imply modes that may resonate quickly or during short events. essential for structural integrity and noise/vibration assessments. The harmonic distortion seen in the stator/rotor data has an indirect effect on the magnetizing branch of the comparable circuit. The effective permeability, which is impacted by harmonic flux, gradually changes the magnetizing reactance. Power factor is typically calculated using the phase difference between voltage and current. However, the phase angle and harmonic content statistics presented here show how power factor may be reduced by non-linear loading and magnetic saturation. Harmonic and modal charts are crucial for identifying structural resonance, rotor/stator imbalance, electromagnetic noise, low power quality, or supply distortion.

V. Conclussion

In order to increase the motor's working lifespan under dynamic loading and thermal stress, this work successfully illustrates the electromagnetic design and thermal modeling of a three-phase induction motor. Using a combination of multi-domain simulations and finite element analysis (FEA), critical performance parameters such as temperature distribution, heat flow, shaft torque, efficiency, slip, and power quality have all been thoroughly investigated. The motor's windings reached a maximum temperature of approximately 93.4°C, which is still below the insulation class B limit of 130°C, indicating safe thermal operation, per the results of the thermal simulation. The overall profile demonstrates efficient heat dissipation, especially with air cooling, despite the presence of isolated hot spots in the axial temperature distribution around the rotor and stator cores Figure.1. The heat flow investigation Figure.2 showed steady-state convergence after 1.5 seconds, with enhanced heat transfer through the stator and rotor yoke surfaces. These results confirm the effectiveness of the cooling approach and reveal few thermal restrictions. The shaft torque Figure 3 demonstrated strong transient performance, maintaining high peaks with minimal variability under dynamic load conditions. The efficiency curve Figure 4, which showed intermittent peaks between 80 and 85% and brief declines caused by load fluctuations, demonstrated a healthy motor under variable loading. The slip performance Figure 6 was within the range of ±0.25 for the majority of the operation, with brief excursions during rapid transients approaching -1. The voltage phase peak Figure 5 maintained projected voltage levels throughout the simulation, supporting voltage stability. The stator and rotor harmonic analysis revealed low-order harmonics, namely the third, fifth, and seventh harmonics, but they were within acceptable ranges. The vibration frequency spectrum Figure 9, which revealed no critical resonance at the working frequency, validated mechanical stability. Additionally, the results of the modal analysis Figure 10 demonstrated a distinct separation between the natural frequencies and the operational frequency range. The lumped stiffness and mass distribution are modified to avoid structural resonance and reduce mechanical wear and vibration-related degradation over time.

In order to forecast and mitigate early deterioration processes, it has proved essential to integrate thermal and electromagnetic modelling. The induction motor's ability to function safely under temperature limitations, preserve mechanical integrity, provide torque efficiently with little slip, and maintain stable performance even under dynamic electrical loads is confirmed by the simulations. Therefore, this study shows that appropriate heat control, material choice, and structural adjustment significantly increase motor longevity, dependability, and energy efficiency, particularly in traction and industrial applications. [18, 19, 20]

References

[1] O. I Okoro, Prolong The Lifespan Of Industrial Electric Machines Through The Development Of Accurate Dynamic And Thermal Model, 53rd Inaugural Lecture Of Michael Okpara University Of Agriculture, Umudike Abia State, Nigeria, 17th April 2024.

[2] Okoro, Ogbonnaya I. "Steady And Transient States Thermal Analysis Of A 7.5-Kw Squirrel-Cage Induction Machine At Rated-Load Operation." Ieee Transactions On Energy Conversion 20, No. 4 (2005): 730-736.

[3] Ejiofor, O. Stephen, Ugwu Justin, N. Damian Benneth, And Ogbuefi Uche. "Development And Thermal Modeling Of An Induction Machine." International Journal Of Engineering & Technology 8, No. 4 (2019), 500-508. 2019

[4] Abdelrahman, S. Ahmed, And Berker Bilgin. "Computationally Efficient Surrogate-Based Magneto-Fluid-Thermal Numerical Coupling Approach For A Water-Cooled Ipm Traction Motor." Ieee Access 10 (2022): 83692-83704. 2022

[5] Hussein, H. M., Ibrahim, A. M., Taha, R. A., Rafin, S. S. H., Abdelrahman, M. S., Kharchouf, I., & Mohammed, O. A. State-Of-The-Art Electric Vehicle Modeling: Architectures, Control, And Regulations. Electronics, 13(17), 3578. 2024

[6] Lusuardi, Luca, A. Cavallini, M. Gomez De La Calle, Juan Manuel Martínez-Tarifa, And G. Robles. "Insulation Design Of Low Voltage Electrical Motors Fed By Pwm Inverters." Ieee Electrical Insulation Magazine 35, No. 3 (2019): 7-15, 2019

[7] Wu, Jinglai, Bing Wang, And Xianqian Hong. "Driving Torque Control Of Dual-Motor Powertrain For Electric Vehicles." In Actuators, Vol. 11, No. 11, P. 320. Mdpi, 2022.

[8] Kim, Dong-Min, Young-Hoon Jung, Kyoung-Soo Cha, And Myung-Seop Lim. "Design Of Traction Motor For Mitigating Energy Consumption Of Light Electric Vehicle Considering Material Properties And Drive Cycles." International Journal Of Automotive Technology 21 (2020): 1391-1399, 2020

[9] Kim, Dong-Min, Soo-Gyung Lee, Dae-Kee Kim, Min-Ro Park, And Myung-Seop Lim. "Sizing And Optimization Process Of Hybrid Electric Propulsion System For Heavy-Duty Vehicle Based On Gaussian Process Modeling Considering Traction Motor Characteristics." Renewable And Sustainable Energy Reviews 161 (2022): 112286, 2022

[10] Wojciechowska, G., Bednarz, Ł.J., Dolińska, N., Opałka, P., Krupa, M. And Imnadze, N. Intelligent Monitoring System For Integrated Management Of Historical Buildings. Buildings (2075-5309), 14(7). 2024
[11] Jung, Ho-Chang, Deok-Jin Kim, Sang-Yong Jung, And Dongsu Lee. "Optimization Method To Maximize Efficiency Map Of A Drive Motor With Electrical Winding Changeover Technique For Hybrid Ev." Ieee Transactions On Applied Superconductivity 30, No. 4 (2020): 1-5, 2020
[12] Tavares, J., Silva, A. And De Brito, J. Computational Models Applied To The Service Life Prediction Of External Thermal Insulation Composite Systems (Etics). Journal Of Building Engineering, 27, P.100944. 2020
[13] Bahgat, B.H., Elhay, E.A., Sutikno, T. And Elkholy, M.M., Revolutionizing Motor Maintenance: A Comprehensive Survey Of State-Of-The-Art Fault Detection In Three-Phase Induction Motors. International Journal Of Power Electronics And Drive Systems, 15(3), Pp.1968-1989. 2024
[14] Hanifi, S., Alkali, B., Lindsay, G., Waters, M. And Mcglinchey, D. Advancements In Predictive Maintenance Modelling For Industrial Electrical Motors: Integrating Machine Learning And Sensor Technologies. Measurement: Sensors, 38, P.101473. 2025
[15] Wallscheid, O. Thermal Monitoring Of Electric Motors: State-Of-The-Art Review And Future Challenges. Ieee Open Journal Of Industry Applications, 2, Pp.204-223. 2023
[16] Bahgat, B.H., Elhay, E.A. And Elkholy, M.M. Advanced Fault Detection Technique Of Three Phase Induction Motor: Comprehensive Review. Discover Electronics, 1(1), P.9. 2024
[17] Yousuf, M., Alsuwian, T., Amin, A.A., Fareed, S. And Hamza, M. Iot-Based Health Monitoring And Fault Detection Of Industrial Ac Induction Motor For Efficient Predictive Maintenance. Measurement And Control, 57(8), Pp.1146-1160. 2024
[18] Szczepanski, M., Malec, D., Maussion, P. And Manfé, P. Design Of Experiments Predictive Models As A Tool For Lifespan Prediction And Comparison For Enameled Wires Used In Low-Voltage Inverter-Fed Motors. Ieee Transactions On Industry Applications, 56(3), Pp.3100-3113. 2020
[19] Arangio, A.M. Novel Methods Of Thermal Management In High-Performance Induction Motors Using Direct Stator Winding Cooling (Master's Thesis, University Of Windsor (Canada)). 2023
[20] Mahale, Manish D., And Bipasa Bimalendu Patra. "Efficient Design, Materials And Specifications Of Electric Motors Used In Electric Vehicle Challenges." In Energy Efficient Vehicles, Pp. 126-155. Crc Press, 2024.